International Journal of Nanomedicine

Dovepress
open access to scientific and medical research

Open Access Full Text Article

ORIGINAL RESEARCH

Gadolinium-doped bioglass scaffolds promote osteogenic differentiation of hBMSC via the Akt/GSK3β pathway and facilitate bone repair in vivo

This article was published in the following Dove Medical Press journal:
International Journal of Nanomedicine

Dao-Yu Zhu[1,*]
Bin Lu[2,*]
Jun-Hui Yin[1]
Qin-Fei Ke[2]
He Xu[2]
Chang-Qing Zhang[1]
Ya-Ping Guo[2]
You-Shui Gao[1,3]

[1]Department of Orthopedic Surgery, Shanghai Jiao Tong University Affiliated Sixth People's Hospital, Shanghai 200233, China; [2]The Education Ministry Key Lab of Resource Chemistry, Shanghai Key Laboratory of Rare Earth Functional Materials, Shanghai Normal University, Shanghai 200234, China; [3]Centre for Orthopaedic Research, Faculty of Health and Medical Sciences, The University of Western Australia, Perth, WA 6009, Australia

*These authors contributed equally to this work

Correspondence: Chang-Qing Zhang
Department of Orthopedic Surgery, Shanghai Jiao Tong University Affiliated Sixth People's Hospital, No 600 Yishan Road, Xuhui District, Shanghai 200233, China
Tel +86 21 6436 9181
Email zhangcq@sjtu.edu.cn

Ya-Ping Guo
The Education Ministry Key Lab of Resource Chemistry, Shanghai Key Laboratory of Rare Earth Functional Materials, Shanghai Normal University, No.100 Guilin Road Shanghai 200234, China
Tel +86 21 6432 2000
Email ypguo@shnu.edu.cn

Background: Biomaterial-induced osteogenesis is mainly related to hierarchically porous structures and bioactive components. Rare earth elements are well known to promote osteogenesis and stimulate bone repair; however, the underlying biological effects of gadolinium (Gd) element on bone regeneration are not yet known.

Methods: In this study, we successfully fabricated gadolinium-doped bioglass (Gd-BG) scaffolds by combining hollow mesoporous Gd-BG microspheres with chitosan and evaluated in vitro effects and underlying mechanisms with Cell Counting Kit-8, scanning electron microscopy, alkaline phosphatase, Alizarin red staining, and polymerase chain reaction. Cranial defect model of rats was constructed to evaluate their in vivo effects.

Results: The results indicated that Gd-BG scaffolds could promote the proliferation and osteogenic differentiation of human bone marrow-derived mesenchymal stem cells (hBMSCs). Mechanistically, the Akt/GSK3β signaling pathway was activated by the Gd-BG scaffolds. The enhancing effect of Gd-BG scaffolds on the osteogenic differentiation of hBMSCs was inhibited by the addition of LY294002, an inhibitor of Akt. Moreover, the in vivo cranial defect model of rats indicated that the Gd-BG scaffolds could effectively promote bone regeneration.

Conclusion: Both in vitro and in vivo results suggested that Gd-BG scaffolds have promising applications in bone tissue engineering.

Keywords: bone scaffold, gadolinium, Akt/GSK3β pathway, bone regeneration

Introduction

Autografts are considered as "gold standard" for the reconstruction of bone defects caused by traumas and bone diseases; however, they have the following disadvantages: limited sources, donor-site morbidity, and second invasive surgery.[1] An alternative strategy is to develop artificial bone scaffolds that provide suitable microenvironments for bone regeneration.[2–6] Porous scaffolds such as bioglass (BG), hydroxyapatite, β-tricalcium phosphate, chitosan (CS), collagen, and poly (lactic-co-glycolic acid) are believed to be biocompatible and osteoconductive materials, which can positively regulate cell–material interactions.[2–6] Present studies focus on improving the osteoinductivity of bone scaffolds in order to effectively reconstruct bone defects.

BG, an admired bone biomaterial, has been used in orthopedic applications since its discovery by Hench et al in 1971.[7] The biodegraded products of BG can provide sufficient PO_4^{3-} and Ca^{2+} ions for the biomineralization of in vivo apatite.[8] The Si element in BG contributes to the differentiation of osteoblast-like cells and calcification of bone tissue under appropriate concentrations.[9,10] In addition, the hierarchically porous characteristics of BG scaffolds play a pivotal role in bone regeneration

submit your manuscript | www.dovepress.com
Dovepress
http://dx.doi.org/10.2147/IJN.S193576

performances.[11,12] The interconnected macroporous architecture facilitates the attachment of cells, diffusion of nutrients, and in-growth of blood vessels and newly formed bones.[11] The mesopores not only provide more active sites for protein adsorption and bone-like apatite formation, but also are useful for drug-delivery application.[12,13] In particular, BG microspheres that combine hollow cores with mesoporous shells provide the hierarchically porous microenvironment for tissue regeneration.[14]

Recently, the incorporation of trace bioactive elements such as Ag, Cu, Sr, and Zn in BG was found to enhance the antibacterial property, osteogenic activity, and angiogenic capacity.[10,15] Incorporation of lanthanide elements into BG have been widely investigated. Lanthanides have been shown to functionally mimic calcium and treat bone density disorders.[16] Addition of CeO_2 nanoparticles to bioactive glass scaffolds could enhance cell proliferation and collagen production in mesenchymal stem cells (MSCs). Lanthanum phosphate could facilitate osteoblast cell adhesion.[17] Gadolinium (Gd), an element of lanthanide, has been widely used as a contrast agent for magnetic resonance imaging (MRI) studies.[18] Many studies have shown a considerably higher level of Gd deposition in bone tissue, indicating that bone might be a preferential site of Gd deposition.[19–22] Thus, Gd-containing biomaterials have attracted considerable interest worldwide.[23,24] The in vitro studies have shown that Gd could promote the proliferation of various kinds of cells.[25–27] Studies on the magnesium alloys incorporated with Gd and Zinc for orthopedic implant showed that Gd possessed properties such as superior mechanical properties and corrosion resistance.[28] Okade et al showed Gd could promote calcium deposition of MSCs.[29] However, the specific effects of Gd combined with BG on bone formation remain unclear. Whether Gd could affect bone metabolism and its underlying mechanism is not yet known.

This study aimed to fabricate Gd-doped BG (Gd-BG) scaffolds and evaluate the effect of Gd on the response of human bone marrow-derived MSCs (hBMSCs) in vitro and on bone regeneration in vivo. The response of hBMSCs cultured with Gd-BG was evaluated using Cell Counting Kit-8 (CCK-8), scanning electron microscopy (SEM), ALP activity, Alizarin red staining (ARS), and PCR. Further, the underlying mechanisms were investigated using Western blot assay. Based on the findings of in vitro studies, we evaluated bone regeneration in rat cranial defects implanted with Gd-BG scaffolds at 8 weeks by using micro-computed tomography (micro-CT), histology, and immunohistochemistry analyses. The results indicated that Gd-BG scaffolds could activate the Akt/GSK3β signaling pathway and lead to enhanced bone regeneration.

Materials and methods

Synthesis of Gd-BG microspheres

BG ($84SiO_2 \cdot 12CaO \cdot 4P_2O_5$) microspheres as control group were prepared by using a self-assembly method. Briefly, cetyltrimethylammonium bromide (CTAB) (0.82 g) was completely dissolved in deionized water (165.0 mL) and ethanol (78.0 mL) mixture under mechanical agitation, followed by addition of $NH_3 \cdot H_2O$ solution (3.00 mL). Tetrahydrate orthosilicate (3.00 mL) was injected into the above mixture and then stirred for 30 minutes. Under the same process conditions, triethylphosphate (0.23 mL) and $Ca(NO_3)_2 \cdot 4H_2O$ (0.64 g) were successively added to the reaction solution. After the reaction was continued for 12 hours, the BG precipitations were filtered, washed with alcohol and water mixture, and dried at 60°C. Finally, the BG microspheres were produced after calcination at 650°C for 3 hours. The Gd-BG microspheres were prepared using the same method except that a part of $Ca(NO_3)_2 \cdot 4H_2O$ was replaced by $Gd(NO_3)_3 \cdot 6H_2O$. The Gd-BG microspheres with Gd/Ca molar ratios of 1:3, 1:5, and 1:7 were abbreviated as Gd1/3-BG, Gd1/5-BG, and Gd1/7-BG microspheres, respectively.

Preparation of Gd-BG scaffolds

CS powder (2.0 g) was completely dissolved in an acetic acid solution (50 mL) under mechanical agitation, followed by addition of Gd-BG microspheres (2.0 g). After the mixture was stirred further for 2 hours, it was injected into a 24-well plate or 96-well plate. The samples were frozen at −20°C and then freeze-driedin a lyophilizer at −80°C for 42 hours. The as obtained Gd-BG/CS scaffolds were soaked in NaOH solution for 24 hours, washed with deionized water until a pH of 7.0 was reached, and freeze-dried again. The BG scaffolds were constructed using the same method. The sizes used for the in vitro study were the same as 24-well plates and the sizes used for in vivo study were the same as 96-well plates. The percentage of Gd in the Gd1/7-BG, Gd1/5-BG, and Gd1/3-BG scaffolds was 2.04 wt%, 2.68 wt%, and 3.94 wt%, respectively.

Characterization

The phases of Gd-BG microspheres and Gd-BG/CS scaffold were characterized by X-ray power diffraction (XRD; D/Max-III). The functional groups of samples were detected by Fourier transform infrared spectroscopy (FTIR; Nicolet 5DX)

by using a KBr pellet technique. The morphologies of the microspheres and scaffolds were characterized by SEM (JSM-6380LV) with energy-dispersive spectrometry. The microstructure of Gd-BG microspheres was detected by transmission electron microscopy (TEM; JEOL2100). N_2 adsorption–desorption isotherms of Gd-BG powders were measured at 77 K by using an automatic surface area and porosity analyzer (AUTOSORB-1-C; Quantachrome). The pore size distribution curve was calculated by the Barrett–Joyner–Halanda (BJH) method. The compressive strengths of cylindrical scaffolds with diameter of 1.5 cm and height of 1.5 cm were tested by microcomputer control electronic universal testing machine (WDW-05C; Shanghai Hualong Test Instruments Corporation) with a compression speed of 5 mm/min. The in vitro release performances of the BG1/3-Gd scaffolds were investigated after the scaffolds were soaked in ultrapure water at 37°C. At different time points, the concentrations of Ca, Si, and Gd ions in the release medium were characterized by using inductively coupled plasma/optical emission Spectrometry (ICP; iCAP 7000; Thermo Fisher Scientific, Waltham, MA, USA).

Cell isolation and culture

The hBMSCs were collected from donors as previously described.[30] Written informed consents in accordance with the Declaration of Helsinki were obtained from each patient. All procedures were approved by the Ethics Review Board of Shanghai Jiao Tong University Affiliated Sixth People's Hospital. The hBMSCs were then cultured with α-minimum essential medium (Thermo Fisher Scientific) supplemented with 10% FBS (Thermo Fisher Scientific), 100 U/mL penicillin (Thermo Fisher Scientific), and 100 μg/mL streptomycin (Thermo Fisher Scientific) at 37°C with 5% CO_2 and 95% humidity. The hBMSCs were passaged when the cells reached 80%–90% confluence. Ionic dissolution was prepared according to the procedures reported in the literature.[31,32] About 1 g of Gd-BG scaffold was soaked in 30 mL of serum-free α-MEM. After incubation for 3 days at 37°C, the mixture was centrifuged, supernatant was collected, filtered through a 0.22 mm filter, and stored at 4°C for future use.

Cell proliferation and adhesion

At passage 3, hBMSCs were seeded on the Gd-BG scaffolds in a 96-well plate. At days 1, 3, and 7, adherent cells were harvested for the determination of cell proliferation by using the CCK-8 kit (Dojindo Molecular Technologies, Inc., Kumamoto, Japan) following manufacturer's recommendations. The absorbance was measured at 450 nm (Bio-Rad 680; Bio-Rad Laboratories, Hercules, CA, USA). The cell viability (%) was calculated according to the following formula:[33]

$$\text{Cell viability (\%)} = \frac{OD_{sample} - OD_{blank}}{OD_{control} - OD_{blank}} \times 100.$$

The hBMSCs morphology on Gd-BG scaffolds was visualized using SEM. The hBMSCs were seeded on Gd-BG scaffolds in 24-well culture plates and allowed to adhere to the scaffolds for 3 days. The samples were then washed three times with PBS and fixed with 2.5% glutaraldehyde overnight. The fixed samples were dehydrated in a graded series of ethanol (30%, 50%, 70%, 90%, and 100%). Next, the samples were freeze-dried for 4 hours at −80°C. Finally, the specimen was coated with gold, and the morphological characteristics of the hBMSCs were observed using SEM (Hitachi S-4700).

ALP activity assays

The hBMSCs were seeded in a 24-well plate at the density of 5×10^5 cells/well with the osteogenic induction supplement containing 10 mM sodium-glycerophosphate, 50 μg/mL ascorbic acid, and 10^{-7} M dexamethasone. A series of concentrations of Gd-BG dissolution were added to the medium. After the cells were cultured for 7 days, the cell layers were washed with PBS for three times and lysed in 200 μL of 0.2% Triton X-100 for 30 minutes. The lysates were sonicated after centrifugation at 14,000 rpm for 15 minutes at 4°C. Next, 50 μL of the supernatant was mixed with 150 μL of the working solution according to manufacturer's protocol (Nanjing Jiancheng Bioengineering Institute, Jiangsu, China). The formation of p-nitrophenol from p-nitrophenylphosphate was evaluated by measuring the absorbance at 405 nm by using a microplate reader (Bio-Rad 680; Bio-Rad Laboratories). The ALP activity was calculated using the ratio of experimental samples to standard and was represented as millimoles of p-nitrophenol produced per minute per milligram of protein.

ALP staining

The hBMSCs were seeded in a 24-well plate at the density of 5×10^6 cells/well. After 24 hours, the medium was changed for osteogenic induction medium with or without different concentrations of Gd-BG dissolution. ALP staining was performed according to manufacturer's instructions (Beyotime, Haimen, China). Briefly, hBMSCs were first washed with

PBS for three times. Next, they were incubated in a mixture of nitro-blue tetrazolium and 5-bromo-4-chloro-3-indolylphosphate for 30 minutes. Subsequently, the cells were viewed under a phase contrast light microscope.

Alizarin red staining

The formation of mineralized matrix nodules was determined using ARS on the 21st day after the hBMSCs were seeded in the 24-well plate with osteogenic induction medium. The cells were washed with PBS for three times, fixed with 4% paraformaldehyde, and then stained with Alizarin red solution (Cyagen Biosciences, Santa Clara, CA, USA) for 15 minutes, according to manufacturer's instructions.

Western blot analysis

Immunoblotting was performed to detect the protein expression of hBMSCs. hBMSCs were treated with different concentrations of Gd-BG dissolution for different time points. Briefly, the cells were washed with PBS and then collected in cell lysis buffer. Protein concentration was determined using the bicinchoninic acid assay kit (Cell Signaling Technology, Danvers, MA, USA). For this, 10 μg of the extract was electrophoresed in 10% sodium dodecyl sulfate–polyacrylamide gels and transferred to polyvinylidene difluoride membranes. The membranes were treated with the relative antibodies. Primary antibodies, including anti-β-catenin, anti-p-Akt, anti-total-Akt, anti-p-GSK3β, and anti-total-GSK3β, were provided by Cell Signaling Technology. The membranes were then incubated with a secondary antibody (Cell Signaling Technology). After chemiluminescence, LEICA DM 4000 was used to detect the target bands. The results were normalized to the loading control (GAPDH; BioTNT, Shanghai, China). All samples were measured in triplicate.

Quantitative RT-PCR

Total mRNA was extracted from hBMSCs after culturing for 3 days by using TRIzol-up (TransGen Biotech). Total RNA was reverse transcribed into cDNA according to manufacturer's instructions (Thermo Fisher Scientific). Reverse transcription PCR was then performed on an ABI 7900 HT Sequence Detection System. The relative expression of the osteoblast markers OCN and BSP was normalized against β-actin. Primers used in this study are listed in Table 1. All samples were measured in triplicate.

Akt inhibitor treatment

The role of Akt/GSK3β pathway in the interaction between Gd-BG and hBMSCs was confirmed by using a selective Akt inhibitor LY294002 (Selleck, Houston, TX, USA). According to the protocol, 10 μM of LY294002 was added to hBMSCs with Gd-BG dissolution.

Animals and surgical procedure

Care and use of laboratory animals were approved by the Animal Research Committee of Shanghai Sixth People's Hospital, Shanghai Jiao Tong University. All animal experiments were performed according to the Animal Management Regulations of China (1988 and revised in 2001, Ministry of Science and Technology). Twenty male SD rats were used to create a cranial bone defect model for the in vivo study, as we previously described.[31] Based on the results of cell culture experiments, we used Gd1/3-BG scaffold as the experiment group, and undoped BG scaffolds were used as control. The animals were anesthetized using intraperitoneal injection of pentobarbital (Nembutal; 3.5 mg/100 g). By using sterile instruments and an aseptic technique, we made a 1.0-cm sagittal incision on the scalp and exposed the cranium by blunt dissection. A full-thickness defect was created in the central area of each parietal bone by using a 5-mm diameter electric trephine (Nouvag AG, Goldach, Switzerland) under constant irrigation with 0.9% saline. The bone defects were divided into two groups and randomly implanted with the Gd1/3-BG scaffolds (n=10) or BG scaffolds (n=10). Following surgery, the soft tissues were repositioned and sutured with 4-0 silk sutures to achieve primary closure. Each animal received an intramuscular injection of antibiotics after surgery. At 8 weeks after surgery, rats were sacrificed with pentobarbital and their cranium tissues were harvested.

Micro-CT

Rat cranium tissues with implants were scanned using micro-CT (Skyscan 1176, Kontich, Belgium). Scanning was performed at a resolution of 18 μm. Experimental settings were as follows: an X-ray voltage of 65 kVp, an anode current

Table 1 Primer sequences used for RT-PCR

Target gene	Forward primer sequence (5′–3′)	Reverse primer sequence (3′–5′)
OCN	CCCCCTCTAGCCTAGGACC	ACCAGGTAATGCCAGTTTGC
BSP	GGGCAGAACCGCATCCAGAGA	GAACGCAGTCGCCGCTTTTTA

Abbreviation: RT-PCR, reverse transcription PCR.

of 385 μA, and an exposure time of 240 ms for each of the 360 rotational steps. Reconstructed images were obtained using 3-D Creator software. The local bone mineral density (BMD) and bone volume to total bone volume (BV/TV) were measured using CTan image analysis.

Sequential fluorescent labeling

At 4 and 6 weeks after surgery, the animals were subjected to an intraperitoneal injection of fluorochromes by using 30 mg/kg Alizarin red (Sigma-Aldrich Co., St Louis, MO, USA) and 5 mg/kg calcein (Sigma-Aldrich Co.). The images of the fluorescent-labeled specimens were captured using a confocal laser scanning microscope (Leica, Heidelberg, Germany). The excitation/emission wavelengths were set as follows: 543/580–670 nm (Alizarin red, red) and 488/500–550 nm (calcium green, green).

Histological analysis

The formalin-fixed samples were decalcified with 10% EDTA (pH =7.2) solution for 4 weeks before they were embedded in paraffin for further histological analysis. Next, 4 μm cross-sections were cut from the middle of the scaffolds and stained with H&E, Van Gieson's (VG) picrofuchsin, and immunohistochemical staining for OCN (Abcam). The images were captured using a Leica DM 4000 microscope.

Statistical analysis

Statistical significance of observed differences between the study groups was determined using SPSS 17.0 software (SPSS, Inc., Chicago, IL, USA) to analyze the data. Values are reported as mean ± SD from separate experiments, each performed in triplicate. Further, *t*-test and single-factor ANOVA was used to assess statistical significance of the results. A value of $P<0.05$ was considered to be statistically significant.

Results

Morphology and structure of Gd-BG scaffolds

The as-obtained Gd-BG particles showed microspheric shapes, having sizes mainly around 300 nm (Figure 1A). Interestingly, hollow cores were detected within the Gd-BG microspheres. The black bright contrasts between the core and shell were detected in the TEM image (Figure 1B), suggesting the presence of hollow structure in the Gd-BG microspheres. In contrast, the microspheres without hollow structure showed the black color in the whole microspheres, as shown in Figure S1. The light spots indicated the presence of disordered mesopores in the microsphere shells. Type IV isotherms of Gd-BG microspheres were observed in Figure 1C, and their type H3 hysteresis loops further showed mesoporous structure. According to the BJH pore size distribution curve, the mesopore sizes of Gd-BG microspheres were around 3.3 nm (Figure 1D). The hierarchically porous Gd-BG microspheres combined the hollow cores with mesoporous shells, resulting in the remarkable pore volume (~0.39 cm^3/g) and Brunauer–Emmett–Teller (BET) surface areas (~312 m^2/g).

The Gd-BG scaffolds were fabricated using a lyophilization method by using the Gd-BG microspheres as the major components and CS as a binding agent. The phase structures of the Gd-BG scaffolds were characterized by the XRD patterns by using pure Gd-BG microspheres as control. BG is known to be a non-crystalline material.[34,35] Only an amorphous peak at $2\theta=20°–30°$ was detected in the Gd-BG microspheres, suggesting that the incorporation of Gd element did not obviously affect the phase structure (Figure 1E). CS, a semi-crystalline material, also showed low crystallinity.[36] The Gd-BG scaffolds, including Gd-BG and CS, showed amorphous characteristic peaks, as shown in the XRD pattern (Figure 1E).

The functional groups of the Gd-BG microspheres and Gd-BG scaffolds were characterized using FTIR spectra (Figure 1F). In the FTIR spectrum of the Gd-BG microspheres, the Si–O–Si vibration bands were located at 1,036 and 1,034 cm^{-1}, and the band due to non-bridging oxygen bonds was detected at 963 cm^{-1}.[37] The bending vibration band of phosphate groups in Gd-BG was located at 608 cm^{-1} (Figure 1F).[38] The Gd-BG scaffolds were hybrid composites of CS and Gd-BG. In addition to those of Gd-BG, the characteristic bands of CS were detected in the FTIR spectrum of Gd-BG scaffolds (Figure 1F). The bands at 895 and 1,559 cm^{-1} corresponded to N–H wagging and $–NH_2$ bending vibration modes, respectively.[39,40] The C–O and bridge oxygen stretching vibration bands were detected at 1,069 and 1,155 cm^{-1}, respectively.[39] The Gd-BG scaffolds also showed characteristic absorption peaks of CH_n groups, including the CH_2 deformation vibration band at 1,418 cm^{-1}, $–CH_3$ symmetric deformation vibration band at 1,384 cm^{-1}, and CH_2 wagging vibration band at 1,335 cm^{-1}.[36] The band at 1,652 cm^{-1} was ascribed to amide I group, and the bands at 1,559 and 1,418 cm^{-1} were ascribed to carboxylate ions.[39] The sharp band at 668 cm^{-1} was attributed to the OCO(δ) vibration of residuary CH_3COOH.[41]

The SEM images of Gd-BG scaffolds showed 3D macropores, with pore sizes of ~150 μm (Figure 2A). The

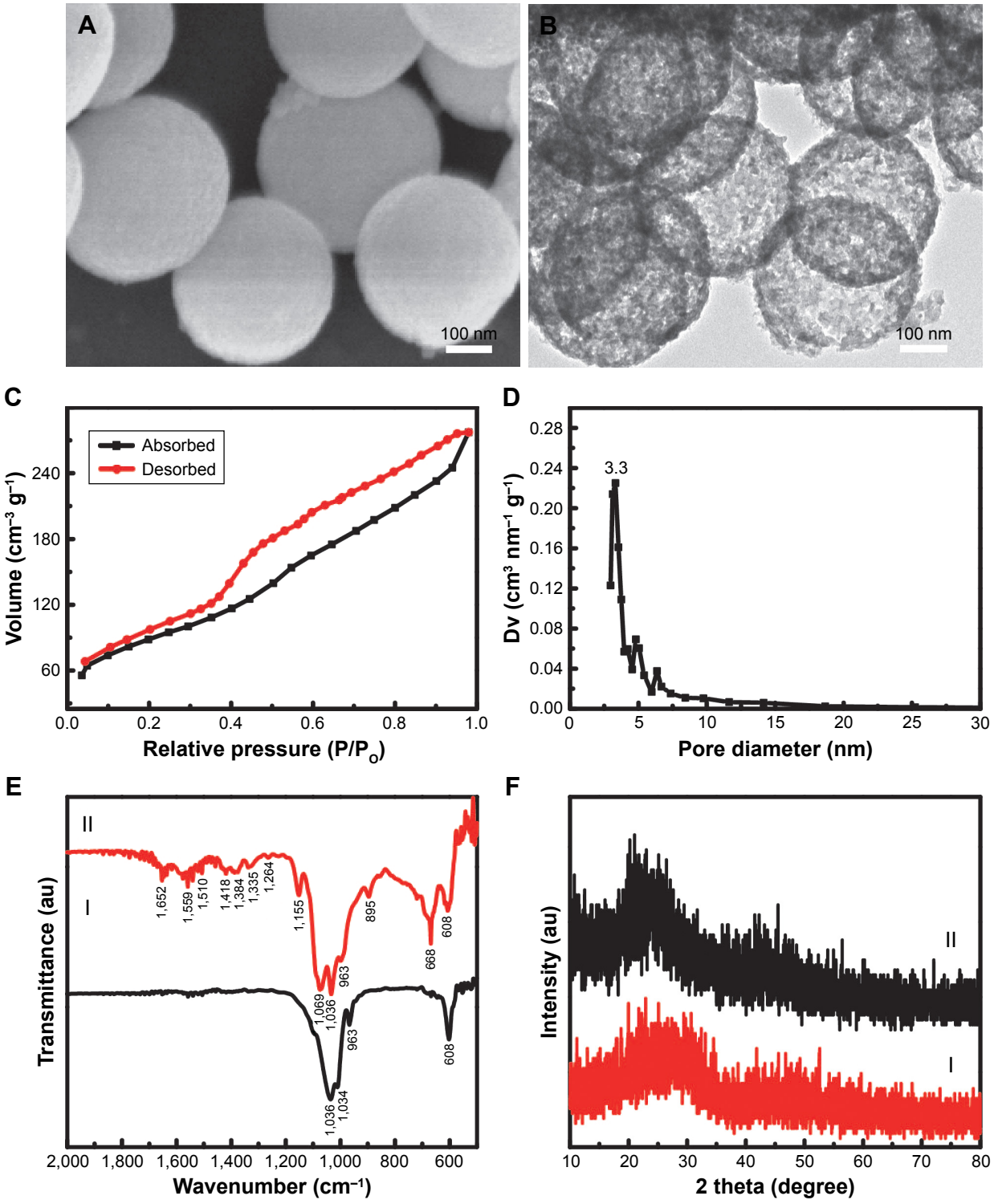

Figure 1 Structural property of Gd-BG scaffold.

Notes: (**A**) SEM image and (**B**) TEM image of Gd-BGS microspheres; (**C**) nitrogen adsorption–desorption isotherm, and (**D**) BJH pore size distribution curve of mesoporous Gd-BGS microspheres. (**E**) The X-ray diffraction patterns of samples: (I) Gd-BG microspheres and (II) Gd-BG scaffolds. (**F**) The Fourier transform infrared spectra of samples: (I) Gd-BG microspheres and (II) Gd-BG scaffolds.

Abbreviations: BJH, Barrett–Joyner–Halenda; Gd-BG, gadolinium-doped bioglass; SEM, scanning electron microscopy; TEM, transmission electron microscopy.

Gd-BG microspheres were uniformly dispersed throughout the pore walls of the scaffolds and were connected together using gel-like CS as the binding agent (Figure 2B). The main components of the Gd-BG scaffolds were Gd-BG and CS, as confirmed by the element distribution maps and energy-dispersive X-ray spectrometry pattern (Figure 2C–F). The Si, Ca, and Gd elements were ascribed to Gd-BG microspheres, and C element was ascribed to CS. The distribution

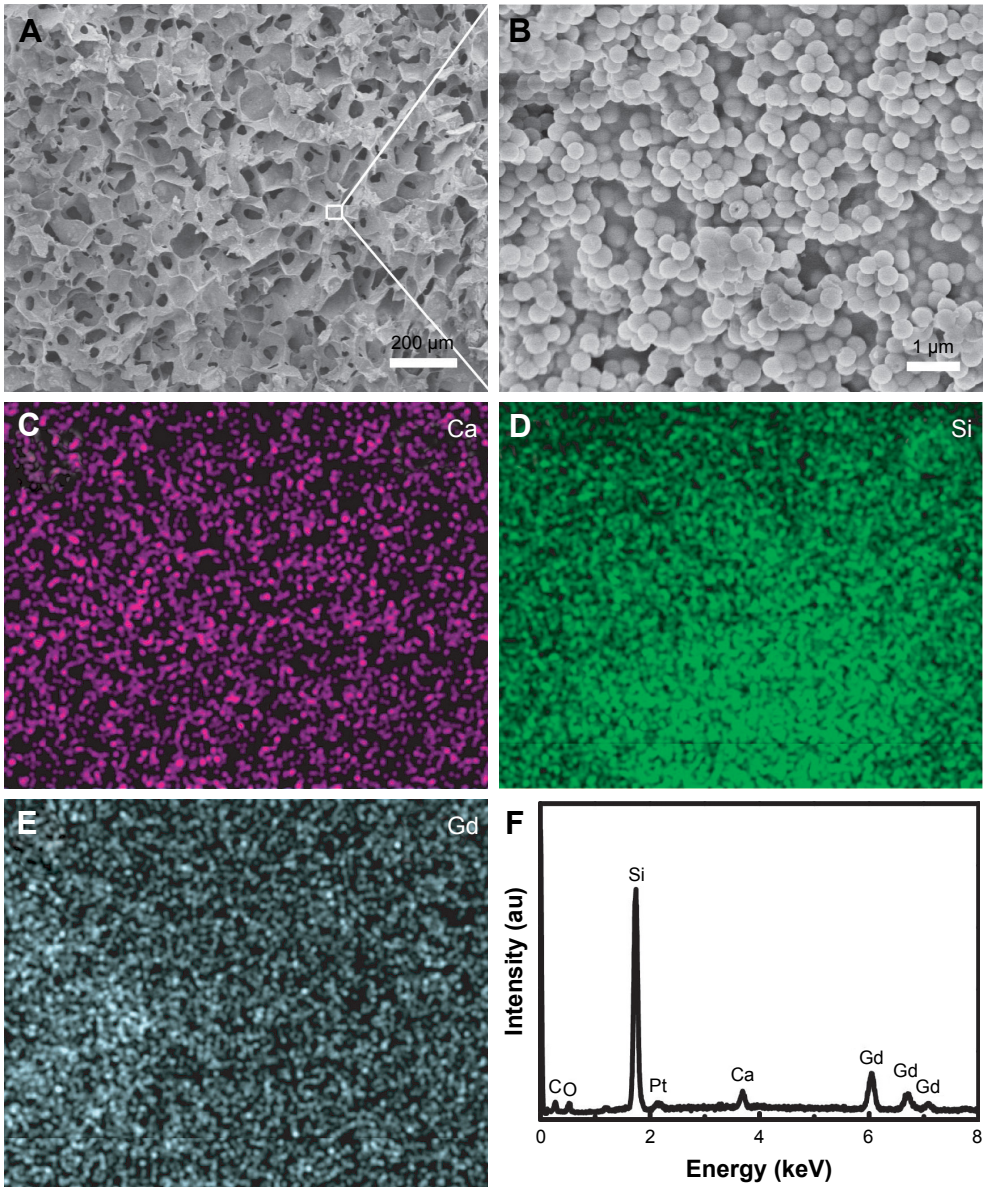

Figure 2 Morphology and chemical composition.
Notes: Characterization of Gd-BG scaffolds: (**A**) low-resolution SEM image; (**B**) high-resolution SEM image; (**C**) Ca element distribution map; (**D**) Si element distribution map; (**E**) Gd element distribution map; and (**F**) energy-dispersive X-ray spectrometry pattern.
Abbreviations: Gd-BG, gadolinium-doped bioglass; SEM, scanning electron microscopy.

maps of Gd, Si, and Ca elements further showed that the Gd-BG microspheres were uniformly dispersed throughout the scaffolds (Figure 2C–E).

Ideal bone scaffolds should not only have a good biological performance, but also possess perfect mechanical properties to fit the surrounding bone tissues. The compression strength of BG scaffolds and BG1/3-Gd scaffolds were tested, as shown in Figure S2A and B. Each sample was tested three times with the same method under the same conditions. As an external force was exerted on these scaffolds, the pore structure of these scaffolds was destroyed initially, and the corresponding stress value to destroy the pore structure of BG scaffolds and BG1/3-Gd scaffolds arrived at 0.11 MPa and 0.13 MPa, respectively, which is in good agreement with the trabecular bone (0.1–0.5 MPa). As shown in Figure S2, these scaffolds were ductile materials, and hence can be pressed tightly with increasing compression; the compression stress that can be sustained by them was more than 1.6 MPa, which can satisfy the demand of bone tissue scaffolds.

The in vitro ion release performances of the BG1/3-Gd scaffolds were tested by soaking the scaffolds in ultrapure water at 37°C. At different time points, the concentrations of Ca, Si, and Gd ions were detected by ICP. Figure S2C and D indicate that all ions were rapidly released from the BG1/3-Gd scaffolds in the initial stage of 24 hours. With the increase of release time, the release rate of Ca, Si, and Gd ions gradually

decreased until a dynamic equilibrium was obtained. After the immersion of the BG1/3-Gd scaffolds in release media for 120 hours, the concentrations of Ca, Si, and Gd ions reached 631.1, 870.9, and 0.37 μM, respectively. The highest concentration of Gd^{3+} was in the safe range for human beings.

Gd-BG scaffolds promote cell viability and osteogenic differentiation of hBMSCs

Cell viabilities of hBMSCs on BG and Gd-BG scaffolds were quantitatively measured using CCK8 assay after culturing for 1, 3, and 7 days. All scaffolds exhibited similar cell viabilities after culturing for 1 day (Figure 3A). On days 3 and 7, the cell viability on Gd-BG scaffolds was significantly higher than that on BG scaffold ($P<0.05$). However, no significant differences were noted between the different concentrations of Gd-BG scaffolds. In addition to cell viabilities, hBMSC morphology on the scaffolds was investigated after culturing for 3 days. Cells adhered and spread well on BG and Gd1/3-BG scaffolds (Figure 3B and C). These results suggested that Gd-BG scaffolds could increase cell viability of hBMSCs while having little impact on their morphology.

The hBMSCs were cultured in osteoinductive medium to compare the effects of Gd-BG and BG on osteogenic differentiation. As an early osteogenic differentiation marker, ALP activity of hBMSCs in Gd-BG dissolution was investigated. Compared to BG dissolution, Gd1/3-BG and Gd1/5-BG dissolution elevated the ALP activity of hBMSCs (Figure 4A). The gene expression results also indicated that hBMSCs in Gd1/3-BG and Gd1/5-BG dissolution had significantly higher level of the osteogenic marker gene, including both OCN and BSP (Figure 4B). ALP staining showed similar results (Figure 4C). However, no significant difference was noted between Gd1/7-BG and BG dissolution. ARS could indicate the mineralization at the late stage of osteogenic differentiation. Considerably more amount of calcium was detected from Gd1/3-BG and Gd1/5-BG dissolution than from BG dissolution and Gd1/7-BG dissolution, as shown by ARS (Figure 4D).

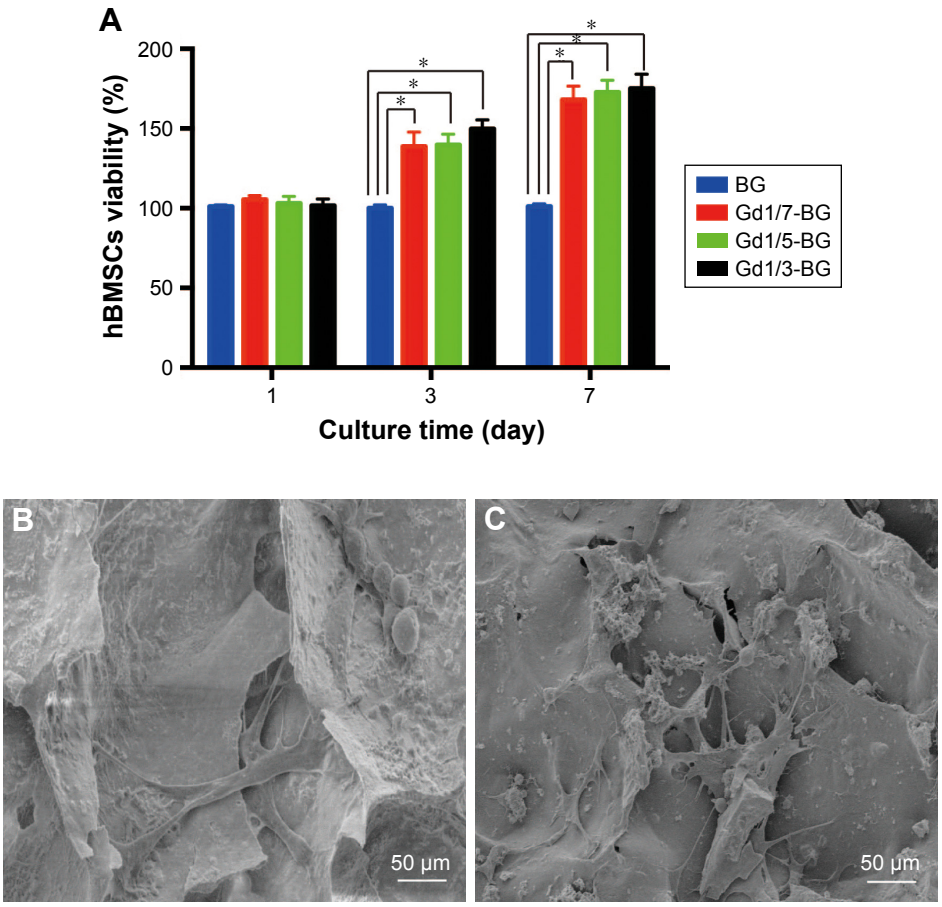

Figure 3 Cell proliferation and adhesion on BG and Gd-BG scaffolds.
Notes: (**A**) Viability of hBMSCs at different concentrations of BG and Gd-BG scaffolds. SEM images showing the attachment of hBMSCs on (**B**) BG and (**C**) Gd1/3-BG. Data are presented as mean ± SD from a representative of three separate experiments performed in quadruplicate (*$P<0.05$).
Abbreviations: Gd-BG, gadolinium-doped bioglass; hBMSC, human bone marrow-derived mesenchymal stem cell; SEM, scanning electron microscopy.

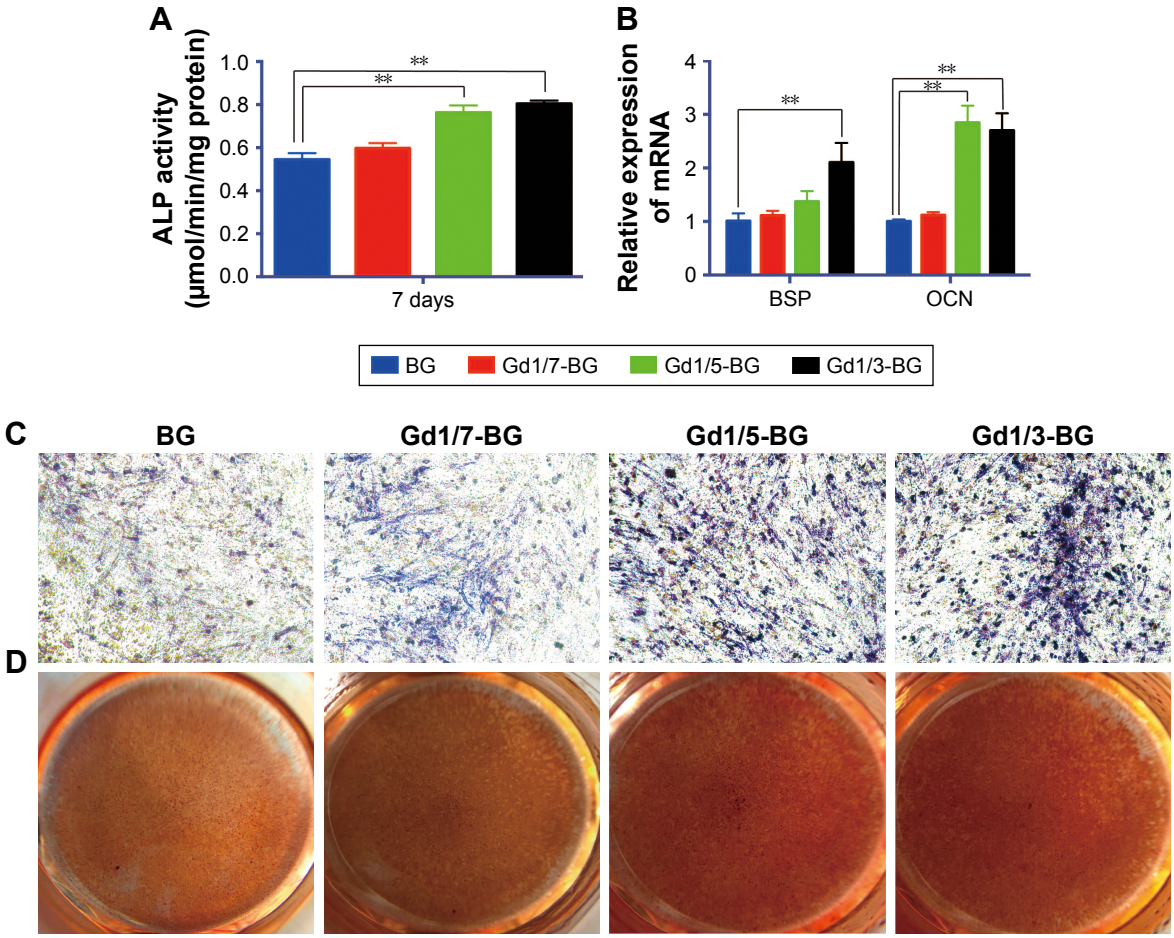

Figure 4 Osteogenic differentiation of hBMSCs in BG and Gd-BG dissolution.
Notes: (**A**) Effects of BG and Gd-BG dissolution on the ALP activity of hBMSCs after culturing for 7 days. (**B**) Osteogenic gene expression of BSP and OCN was detected after hBMSCs were treated with BG and Gd-BG dissolution for 3 days. (**C**) ALP staining showed osteogenic differentiation of hBMSCs treated with BG and Gd-BG dissolution for 14 days (40×). (**D**) Alizarin red staining showing the mineralization of hBMSCs treated with BG and Gd-BG dissolution for 21 days. Data are presented as mean ± SD from a representative of three separate experiments performed in quadruplicate (**$P<0.01$).
Abbreviations: Gd-BG, gadolinium-doped bioglass; hBMSC, human bone marrow-derived mesenchymal stem cell.

Gd-BG scaffolds promote osteogenic differentiation of hBMSCs via Akt/GSK3β pathway

The stimulatory effects of Gd-BG on osteogenic differentiation led us to further investigate the involvement of Akt/GSK3β pathway in this process. The expression of Akt, GSK3β, and β-catenin was examined using Western blot. The phosphorylated Akt and GSK3β of hBMSCs treated with Gd1/3-BG and Gd1/5-BG dissolution for 3 hours was elevated, whereas BG and Gd1/7-BG dissolution had no obvious influence on it (Figure 5A). Total Akt and GSK3β were not changed. β-catenin was detected after hBMSCs were incubated in Gd-BG dissolution for 24 hours. The results showed that Gd1/3-BG and Gd1/5-BG dissolution could increase the level of β-catenin (Figure 5B). The mechanism of Gd-BG was further confirmed by adding the inhibitor of Akt, LY294002. LY294002 decreased the phosphorylated level of Akt and GSK3β, which was enhanced by Gd1/3-BG dissolution (Figure 5C). β-catenin was also decreased by LY294002 (Figure 5D). Quantitative analysis of Western blot has been shown in Figure 5E and F. Consistently, ALP activity, ALP staining, and ARS indicated that the up-regulated osteogenic differentiation of hBMSCs treated with Gd1/3-BG dissolution was decreased by LY294002 (Figure 5G–I). These results collectively indicated that the stimulatory effect of Gd-BG on osteogenic differentiation was partially via the activation of the Akt/GSK3β pathway.

Gd-BG scaffolds promote bone regeneration in rat cranial defect model

The influence of scaffolds on new bone formation in vivo was investigated by implanting the BG and Gd1/3-BG scaffolds into rat critical-sized cranial bone defects. Reconstructed

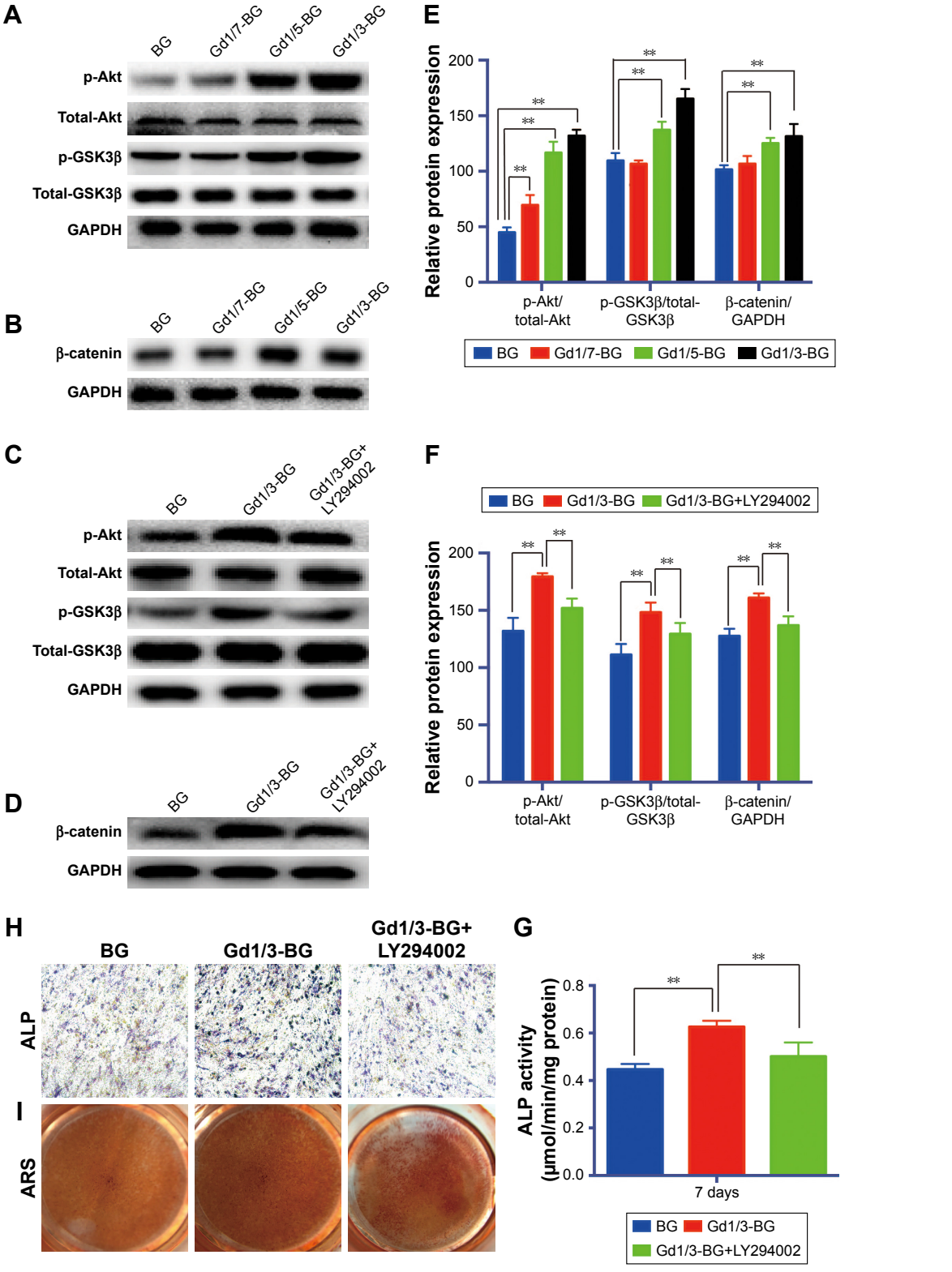

Figure 5 Activation of Akt/GSK3β pathway by Gd-BG.

Notes: (**A**) Western blotting analysis of p-Akt, total-Akt, p-GSK3β, and total-GSK3β for hBMSCs after treatment with different concentrations of Gd-BG dissolution for 3 hours. GAPDH was used as the loading control. (**B**) Western blotting analysis of β-catenin for hBMSCs after treatment with different concentrations of Gd-BG dissolution for 24 hours. (**C**) Western blotting analysis of p-Akt, total-Akt, p-GSK3β, and total-GSK3β for hBMSCs after treatment with BG, Gd1/3-BG dissolution, and Gd1/3-BG dissolution+ LY294002 for 3 hours. (**D**) Western blotting analysis of β-catenin for hBMSCs after treatment with BG, Gd1/3-BG dissolution, and Gd1/3-BG dissolution+ LY294002 for 24 hours. (**E**, **F**) Analysis of protein expression in hBMSCs. (**G**) Effects of BG, Gd1/3-BG dissolution, and Gd1/3-BG dissolution+ LY294002 on the ALP activity of hBMSCs after culturing for 7 days. (**H**) ALP staining showed the osteogenic differentiation of hBMSCs after treatment with BG, Gd1/3-BG dissolution, and Gd1/3-BG dissolution+ LY294002 for 14 days (40×). (**I**) Alizarin red staining showed the mineralization of hBMSCs after treatment with BG, Gd1/3-BG dissolution, and Gd1/3-BG dissolution+ LY294002 for 21 days. Data are presented as mean ± SD from a representative of three separate experiments performed in quadruplicate (**$P<0.01$).

Abbreviations: ARS, Alizarin red staining; Gd-BG, gadolinium-doped bioglass; hBMSC, human bone marrow-derived mesenchymal stem cell.

micro-CT images of cranial defects are shown in Figure 6A. The images showed a higher number of new bone in the defects implanted with Gd1/3-BG scaffolds. Quantitative analysis indicated that the BMD in the Gd1/3-BG scaffolds was significantly higher than that in the BG scaffolds. The BV/TV ratio showed a trend similar to BMD (Figure 6B and C).

Fluorochrome labeling analysis showed amount of bone formation. After 4 weeks, Alizarin red (red) deposited onto

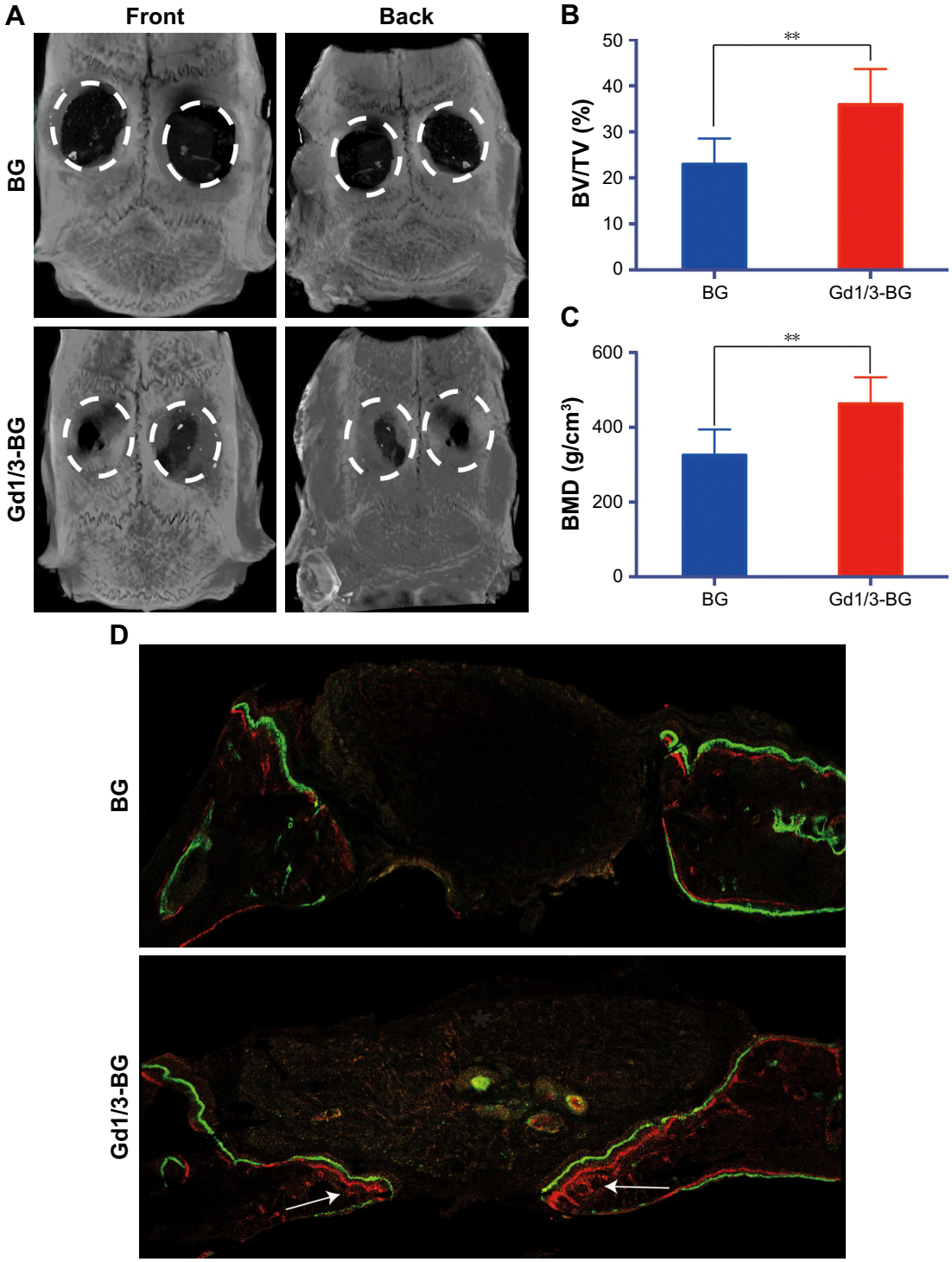

Figure 6 Micro-CT of rat cranial defects implanted with BG and Gd1/3-BG scaffolds at 8 weeks after implantation.
Notes: (**A**) The images of reconstruction of micro-CT for the bone regeneration of the defect area at week 8. (**B**, **C**) BMD and BV/TV in the defects implanted with the Gd1/3-BG and BG scaffolds. Data are presented as mean ± SD from a representative of ten separate experiments (**$P<0.01$). (**D**) New bone formation and mineralization measured histomorphometrically by using fluorochrome labeling analysis in rat cranial defects implanted with Gd1/3-BG and BG scaffolds. White arrow indicates the new bone formation. Alizarin red (red) and calcein (green) were intraperitoneally injected at weeks 4 and 6, respectively.
Abbreviations: BMD, bone mineral density; BV/TV, bone volume to total bone volume; CT, computed tomography; Gd-BG, gadolinium-doped bioglass.

Gd1/3-BG scaffolds in a broader area than on BG scaffolds, exhibiting more intense and extensive red fluorescence. Furthermore, calcein (6 weeks) showed similar results (Figure 6D).

The deposition of new bone tissue was higher in defects implanted with the Gd1/3-BG scaffolds than in those implanted with the BG scaffolds at 8 weeks, which is indicated in the images of decalcified sections stained with H&E and VG picrofuchsin (Figure 7). Immunohistochemical staining for OCN showed that positive area of OCN was greater in Gd1/3-BG scaffolds. These results indicated that Gd1/3-BG scaffolds had significantly better capacity to heal rat cranial defects than BG scaffolds.

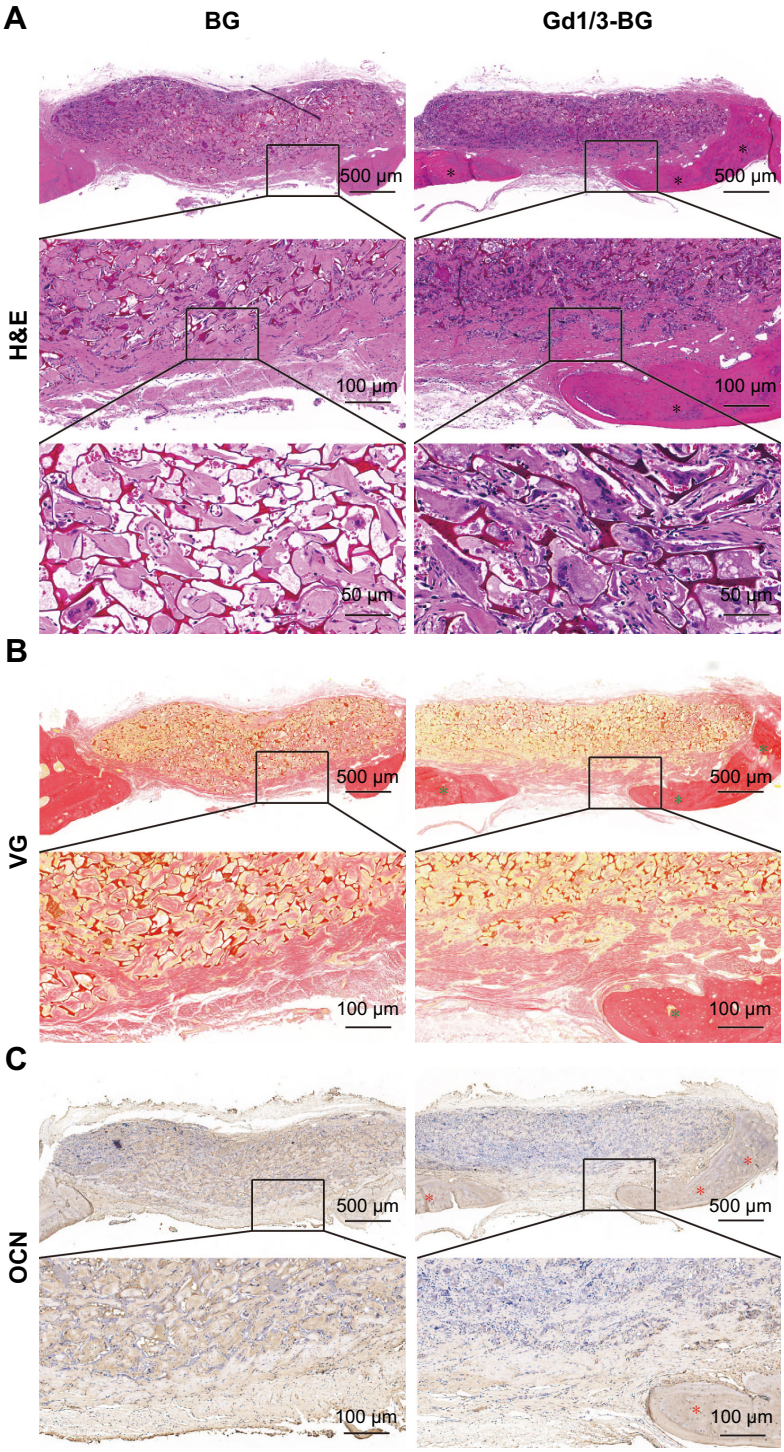

Figure 7 Histological analysis of cranial bone defects.
Notes: (A) H&E, (**B**) VG, and (**C**) immunohistochemical staining of OCN in the defects implanted with Gd-BG and BG scaffolds at 8 weeks after implantation. Black stars indicate new bone formation. Green star indicates new collagen formation, and red stars indicate positive staining of OCN.
Abbreviation: Gd-BG, gadolinium-doped bioglass; VG, Van Gieson's.

Discussion

The bone regeneration capacity of artificial biomaterials depends mainly on cell–material interactions.[2–6] Numerous studies have revealed that hierarchically porous characteristics and bioactive components could effectively regulate cellular performances such as attachment, migration, proliferation, and differentiation.[10–15] In particular, Gd element is found in human bones and plays a key role in bone tissue growth and regeneration.[19–22] In this study, we successfully fabricated Gd-BG scaffolds with hierarchical pores and bioactive Gd element for effective bone defect healing.

The self-assembly method was used to prepare monodisperse Gd-BG microspheres according to the following steps: 1) formation of O/W emulsion system after dissolving CTAB in alcohol water mixtures; 2) self-assembly deposition of Gd-BG precursors on the microemulsion surfaces under the catalysis of $NH_3 \cdot H_2O$; and 3) fabrication of Gd-BG microspheres after calcination removal of organic templates (Figure 1A and B). Mesoporous BGs have thus far been widely studied for bone regeneration.[11,12] The mesopores could increase ion exchange with the surrounding fluids in human bodies, mainly of Ca^{2+} by H^+.[16] The dissolution products of BGs, including Ca, Si, and P elements, have an upregulation effect on pro-osteoblastic genes.[8] Moreover, the hollow cores and mesoporous shells of BG microspheres remarkably increased the surface areas, thereby providing considerably more active sites for bone-like apatite deposition and bone mineralization (Figure 7). In addition to mesoporous structure, macropores play a pivotal role in promoting bone regeneration. In this study, three-dimensionally interconnected microporous Gd-BG scaffolds were created using freeze-drying treatment, in which the hollow mesoporous Gd-BG microspheres were combined with CS (Figure 2). The macroporous structure in the scaffolds could facilitate the attachment and migration of hBMSCs from scaffold surfaces to interiors. The hBMSCs spread well in the macroporous structure, as revealed in the SEM image (Figure 3B andC). Moreover, the section staining images indicated that newly formed bones could grow into scaffolds along the interconnected macrochannels (Figures 6 and 7).

The hollow mesoporous BG scaffolds showed excellent biocompatibility, but their bone regeneration capacity could not effectively heal critical-sized bone defects (Figures 3 and 6). The osteoinductivity was improved by incorporating Gd element in the BG microspheres/scaffolds (Figures 1 and 2). CCK-8 assay results indicated that the Gd-BG scaffolds could promote cell proliferation compared to the pure BG scaffolds, which was in good agreement with the findings of previous studies.[27] Moreover, the differentiation of hBMSCs into osteoblasts is a key step for osteogenesis. ALP activity is an early phenotypic marker for osteogenic differentiation of hBMSCs. Mineralized nodule formation is a phenotypic marker for the last stage of mature osteoblasts. Therefore, the effect of Gd-BG dissolution on osteogenic differentiation of hBMSCs was determined by measuring their ALP activity, ARS, and osteogenic gene expression levels. The in vivo results also showed better bone regeneration in Gd-BG group. Taken together, these results suggest that Gd-BG scaffolds could provide better osteoinductivity for bone regeneration.

The hBMSCs have attracted considerable attention in tissue engineering because of their capability to differentiate into osteoblasts.[42] Numerous studies have shown the critical involvement of the Wnt signaling pathway in the commitment of pluripotent stem cells to the osteoblast lineage.[43–47] β-catenin, which plays a role as a central signaling mediator of the Wnt signaling pathway, could be degraded by the destroy complex. Moreover, GSK3β, a critical protein of the destroy complex, plays a role as a crossroad and could be regulated by many upstream signaling pathways, including the Akt signaling pathway. The activation of the Akt signaling pathway might inactivate GSK3β by phosphorylating Ser9 of GSK3β, which results in the accumulation and translocation of β-catenin, thereby mediating the regeneration of bone. Whether the Akt/GSK3β signaling pathway is involved in the Gd-BG–hBMSCs interaction was determined by conducting Western blot analyses. The results showed that rapid upregulation of Akt/GSK3β signaling pathway occurred in response to Gd-BG dissolution. Further, treatment with small molecule inhibitor of the Akt/GSK3β signaling pathway led to the inhibition of ALP activity and ARS. These data together showed that Gd-BG activated the Akt/GSK3β signaling pathway, and thus triggered the osteogenic differentiation of hBMSCs (Figure 8).

Gd is a paramagnetic lanthanide heavy metal. Its free ionic form (Gd^{3+}) can compete with Ca^{2+} and become toxic in biological systems. Gd could deposit in the brain and induce persistent T1 shortening in deep gray matter structures in subjects with normal renal function. After administration, Gd is eliminated from the body through the urinary and biliary system. They are usually cleared from the blood in about 1.5 hours, and completely recovered from the urine in 7 days (>90% in the first 12 hours).[48–50] However, the concentrations used in this study are far less than the concentrations which could be toxic. Growing evidence supports the hypothesis that Gd-containing contrast agents (0.05–0.2 mmol/kg) used for MRI could trigger the development of nephrogenic systemic fibrosis (NSF).[51] NSF is clinically characterized

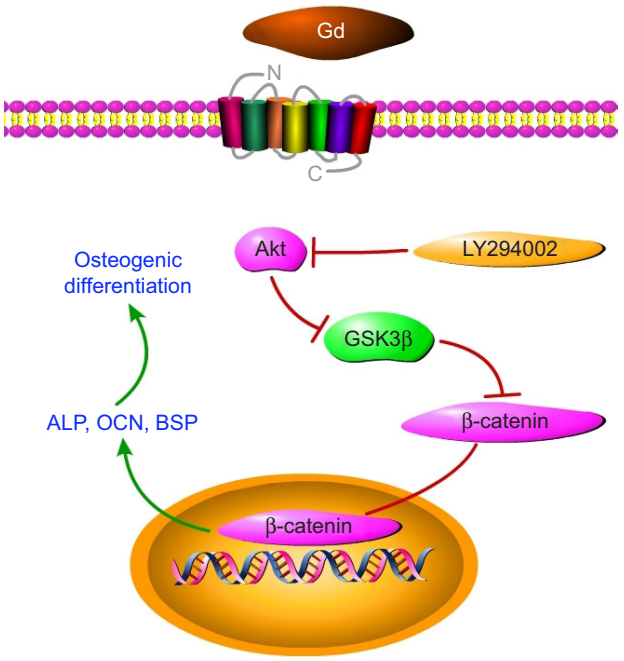

Figure 8 Gd and Akt/GSK3β signaling pathway, where Gd could activate Akt.
Notes: Phosphorylated Akt could prevent GSK3β from forming a complex with β-catenin, resulting in the accumulation of β-catenin. Thus, it could promote osteogenic gene expression and enhance osteogenic differentiation.
Abbreviation: Gd, gadolinium.

by the acute onset of the hardening and thickening of the skin on the extremities and trunk, often resulting in flexion contractures. Recently, a spectrum of abnormal calcifications such as dystrophic calcinosis cutis, benign nodular calcifications, metastatic calcinosis cutis, and osseous metaplasia has been shown to develop in NSF patients.[52,53] Although Gd-BG scaffolds have been shown to be very useful in biomedical and tissue engineering, questions as to whether Gd-BG scaffolds could cause NSF in the human body still remain. Furthermore, the mechanism by which Gd-BG activates Akt/GSK3β signaling pathway needs to be investigated.

Conclusion

We successfully fabricated Gd-BG scaffolds with hierarchical porous structures and bioactive Gd element. At the concentrations used, the incorporation of Gd into bioactive glass scaffolds exhibited good biocompatibility, which not only promoted the proliferation of hBMSCs, but also improved osteoinductivity. The activity of ALP, deposition of minerals, and expression of osteogenic-related genes (*OCN* and *BSP*) increased significantly in hBMSCs treated with Gd-BG scaffolds. When implanted for 8 weeks in rat cranial defects, the Gd-BG scaffolds remarkably enhanced bone regeneration compared to the BG scaffolds. Doping bioactive glass scaffolds with Gd could provide a promising approach for enhancing their capacity to heal bone defects.

Acknowledgment

The current research was supported in part by the National Natural Science Foundation of China (grant no. 81672143).

Disclosure

The authors report no conflicts of interest in this work.

References

1. Maletis GB, Chen J, Inacio MCS, Love RM, Funahashi TT. Increased risk of revision after anterior cruciate ligament reconstruction with bone-patellar tendon-bone allografts compared with autografts. *Am J Sports Med*. 2017;45(6):1333–1340.
2. Lai Y, Cao H, Wang X, et al. Porous composite scaffold incorporating osteogenic phytomolecule icariin for promoting skeletal regeneration in challenging osteonecrotic bone in rabbits. *Biomaterials*. 2018;153:1–13.
3. Liao J, Tian T, Shi S, et al. The fabrication of biomimetic biphasic CAN-PAC hydrogel with a seamless interfacial layer applied in osteochondral defect repair. *Bone Res*. 2017;5:17018.
4. Munir N, Callanan A. Novel phase separated polycaprolactone/collagen scaffolds for cartilage tissue engineering. *Biomed Mater*. 2018;13(5):051001.
5. Quinlan E, López-Noriega A, Thompson E, Kelly HM, Cryan SA, O'Brien FJ. Development of collagen-hydroxyapatite scaffolds incorporating PLGA and alginate microparticles for the controlled delivery of rhBMP-2 for bone tissue engineering. *J Control Release*. 2015;198:71–79.
6. Miguez-Pacheco V, Hench LL, Boccaccini AR. Bioactive glasses beyond bone and teeth: emerging applications in contact with soft tissues. *Acta Biomater*. 2015;13:1–15.
7. Hench LL, Splinter RJ, Allen WC, Greenlee TK. Bonding mechanisms at the interface of ceramic prosthetic materials. *J Biomed Mater Res*. 1971;5:117–141.
8. Kang MS, Lee NH, Singh RK, et al. Nanocements produced from mesoporous bioactive glass nanoparticles. *Biomaterials*. 2018;162:183–199.
9. Obata A, Iwanaga N, Terada A, Jell G, Kasuga T. Osteoblast-like cell responses to silicate ions released from 45S5-type bioactive glass and siloxane-doped vaterite. *J Mater Sci*. 2017;52(15):8942–8956.
10. Hoppe A, Güldal NS, Boccaccini AR. A review of the biological response to ionic dissolution products from bioactive glasses and glass-ceramics. *Biomaterials*. 2011;32(11):2757–2774.
11. Erasmus EP, Sule R, Johnson OT, Massera J, Sigalas I. In vitro evaluation of porous borosilicate, borophosphate and phosphate bioactive glasses scaffolds fabricated using foaming agent for bone regeneration. *Sci Rep*. 2018;8(1):3699.
12. Yan X, Yu C, Zhou X, Tang J, Zhao D. Highly ordered mesoporous bioactive glasses with superior in vitro bone-forming bioactivities. *Angew Chem Int Ed Engl*. 2004;43(44):5980–5984.
13. Yin C, Jia X, Miron RJ, et al. Setd7 and its contribution to boron-induced bone regeneration in Boron-mesoporous bioactive glass scaffolds. *Acta Biomater*. 2018;73:522–530.
14. Wang Y, Chen X. Facile synthesis of hollow mesoporous bioactive glasses with tunable shell thickness and good monodispersity by microemulsion method. *Mater Lett*. 2017;189:325–328.
15. Douglas TEL, Dziadek M, Gorodzha S, et al. Novel injectable gellan gum hydrogel composites incorporating Zn- and Sr-enriched bioactive glass microparticles: high-resolution X-ray microcomputed tomography, antibacterial and in vitro testing. *J Tissue Eng Regen Med*. 2018;12(6):1313–1326.
16. Shi M, Xia L, Chen Z, et al. Europium-doped mesoporous silica nanosphere as an immune-modulating osteogenesis/angiogenesis agent. *Biomaterials*. 2017;144:176–187.

17. Ergun C, Liu H, Webster TJ. Osteoblast adhesion on novel machinable calcium phosphate/lanthanum phosphate composites for orthopedic applications. *J Biomed Mater Res A*. 2009;89(3):727–733.
18. Ramalho J, Ramalho M, Jay M, Burke LM, Semelka RC. Gadolinium toxicity and treatment. *Magn Reson Imaging*. 2016;34(10):1394–1398.
19. White GW, Gibby WA, Tweedle MF. Comparison of Gd(DTPA-BMA) (Omniscan) versus Gd(HP-DO3A) (ProHance) relative to gadolinium retention in human bone tissue by inductively coupled plasma mass spectroscopy. *Invest Radiol*. 2006;41(3):272–278.
20. Tweedle MF, Wedeking P, Kumar K. Biodistribution of radiolabeled, formulated gadopentetate, gadoteridol, gadoterate, and gadodiamide in mice and rats. *Invest Radiol*. 1995;30(6):372–380.
21. Darrah TH, Prutsman-Pfeiffer JJ, Poreda RJ, Ellen Campbell M, Hauschka PV, Hannigan RE. Incorporation of excess gadolinium into human bone from medical contrast agents. *Metallomics*. 2009;1(6):479–488.
22. Tedeschi E, Caranci F, Giordano F, Angelini V, Cocozza S, Brunetti A. Gadolinium retention in the body: what we know and what we can do. *Radiol Med*. 2017;122(8):589–600.
23. Guo Y, Liu W, Ma S, et al. A preliminary study for novel use of two Mg alloys (WE43 and Mg3Gd). *J Mater Sci Mater Med*. 2016;27(5):82.
24. Usman MS, Hussein MZ, Fakurazi S, Ahmad Saad FF. Gadolinium-based layered double hydroxide and graphene oxide nano-carriers for magnetic resonance imaging and drug delivery. *Chem Cent J*. 2017;11(1):47.
25. Fu LJ, Li JX, Yang XG, Wang K. Gadolinium-promoted cell cycle progression with enhanced S-phase entry via activation of both ERK and PI3K signaling pathways in NIH 3T3 cells. *J Biol Inorg Chem*. 2009;14(2):219–227.
26. Li JX, Liu JC, Wang K, Yang XG. Gadolinium-containing bioparticles as an active entity to promote cell cycle progression in mouse embryo fibroblast NIH3T3 cells. *J Biol Inorg Chem*. 2010;15(4):547–557.
27. Shen L, Yang A, Yao P, et al. Gadolinium promoted proliferation in mouse embryo fibroblast NIH3T3 cells through Rac and PI3K/Akt signaling pathways. *Biometals*. 2014;27(4):753–762.
28. Bian D, Deng J, Li N, et al. In vitro and in vivo studies on biomedical magnesium Low-Alloying with elements gadolinium and zinc for orthopedic implant applications. *ACS Appl Mater Interfaces*. 2018;10(5):4394–4408.
29. Okada E, Yamanaka M, Ishikawa O. New insights into the mechanism of abnormal calcification in nephrogenic systemic fibrosis – gadolinium promotes calcium deposition of mesenchymal stem cells and dermal fibroblasts. *J Dermatol Sci*. 2011;62(1):58–63.
30. Chen YX, Zhu R, Ke QF, Gao YS, Zhang CQ, Guo YP. MgAl layered double hydroxide/chitosan porous scaffolds loaded with PFTα to promote bone regeneration. *Nanoscale*. 2017;9(20):6765–6776.
31. Li H, Chang J. Stimulation of proangiogenesis by calcium silicate bioactive ceramic. *Acta Biomater*. 2013;9(2):5379–5389.
32. Li H, Xue K, Kong N, Liu K, Chang J. Silicate bioceramics enhanced vascularization and osteogenesis through stimulating interactions between endothelia cells and bone marrow stromal cells. *Biomaterials*. 2014;35(12):3803–3818.
33. Yang K, Cao W, Hao X, et al. Metallofullerene nanoparticles promote osteogenic differentiation of bone marrow stromal cells through BMP signaling pathway. *Nanoscale*. 2013;5(3):1205–1212.
34. Zhou D, Qi C, Chen YX, et al. Comparative study of porous hydroxyapatite/chitosan and whitlockite/chitosan scaffolds for bone regeneration in calvarial defects. *Int J Nanomedicine*. 2017;12:2673–2687.
35. Lian H, Meng Z. Fabrication, characterization and osteoblast responses of poly (octanediol citrate)/bioglass nanofiber composites. *Mater Sci Eng C Mater Biol Appl*. 2018;84:123–129.
36. Chen Y, Yu J, Ke Q, Gao Y, Zhang C, Guo Y. Bioinspired fabrication of carbonated hydroxyapatite/chitosan nanohybrid scaffolds loaded with TWS119 for bone regeneration. *Chem Eng J*. 2018;341:112–125.
37. Khoshakhlagh P, Rabiee SM, Kiaee G, et al. Development and characterization of a bioglass/chitosan composite as an injectable bone substitute. *Carbohydr Polym*. 2017;157:1261–1271.
38. Chen W, Long T, Guo YJ, Zhu ZA, Guo YP. Magnetic hydroxyapatite coatings with oriented nanorod arrays: hydrothermal synthesis, structure and biocompatibility. *J Mater Chem B*. 2014;2(12):1653–1660.
39. Mauricio-Sánchez RA, Salazar R, Luna-Bárcenas JG, Mendoza-Galván A. FTIR spectroscopy studies on the spontaneous neutralization of chitosan acetate films by moisture conditioning. *Vib Spec*. 2018;94:1–6.
40. Branca C, D'Angelo G, Crupi C, et al. Role of the OH and NH vibrational groups in polysaccharide-nanocomposite interactions: a FTIR-ATR study on chitosan and chitosan/clay films. *Polymer*. 2016;99:614–622.
41. Wilmshurst JK. Infrared investigation of acetic acid and acetic acid-d vapors and a vibrational assignment for the monomeric acids. *J Chem Phys*. 1956;25(6):1171–1173.
42. Maurin AC, Chavassieux PM, Frappart L, Delmas PD, Serre CM, Meunier PJ. Influence of mature adipocytes on osteoblast proliferation in human primary cocultures. *Bone*. 2000;26(5):485–489.
43. Rudnicki MA, Williams BO. Wnt signaling in bone and muscle. *Bone*. 2015;80:60–66.
44. Baron R, Kneissel M. Wnt signaling in bone homeostasis and disease: from human mutations to treatments. *Nat Med*. 2013;19(2):179–192.
45. Liu Z, Jiang H, Dong K, et al. Different concentrations of glucose regulate proliferation and osteogenic differentiation of osteoblasts via the PI3 kinase/Akt pathway. *Implant Dent*. 2015;24(1):83–91.
46. Ying X, Chen X, Liu H, et al. Silibinin alleviates high glucose-suppressed osteogenic differentiation of human bone marrow stromal cells via antioxidant effect and PI3K/Akt signaling. *Eur J Pharmacol*. 2015;765:394–401.
47. You L, Gu W, Chen L, Pan L, Chen J, Peng Y. MiR-378 overexpression attenuates high glucose-suppressed osteogenic differentiation through targeting CASP3 and activating PI3K/Akt signaling pathway. *Int J Clin Exp Pathol*. 2014;7(10):7249–7261.
48. Ramalho J, Ramalho M, Jay M, Burke LM, Semelka RC. Gadolinium toxicity and treatment. *Magn Reson Imaging*. 2016;34(10):1394–1398.
49. Murata N, Murata K, Gonzalez-Cuyar LF, Maravilla KR. Gadolinium tissue deposition in brain and bone. *Magn Reson Imaging*. 2016;34(10):1359–1365.
50. Ramalho J, Ramalho M. Gadolinium deposition and chronic toxicity. *Magn Reson Imaging Clin N Am*. 2017;25(4):765–778.
51. Grobner T. Gadolinium – a specific trigger for the development of nephrogenic fibrosing dermopathy and nephrogenic systemic fibrosis? *Nephrology Dial Transplant*. 2006;21(4):1104–1108.
52. Song J, Volkov S, Shea CR, et al. Nephrogenic systemic fibrosis associated with stromal and vascular calcification, report of two cases. *J Cutan Pathol*. 2009;36(Suppl 1):31–34.
53. Nagai Y, Hasegawa M, Shinmi K, et al. Nephrogenic systemic fibrosis with multiple calcification and osseous metaplasia. *Acta Derm Venereol*. 2008;88(6):597–600.

Supplementary materials

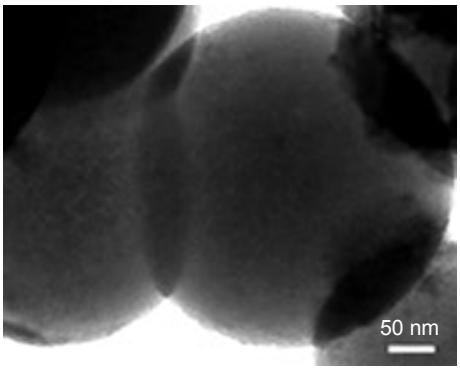

Figure S1 TEM image of BG microspheres without hollow structure.
Abbreviations: BG, bioglass; TEM, transmission electron microscopy.

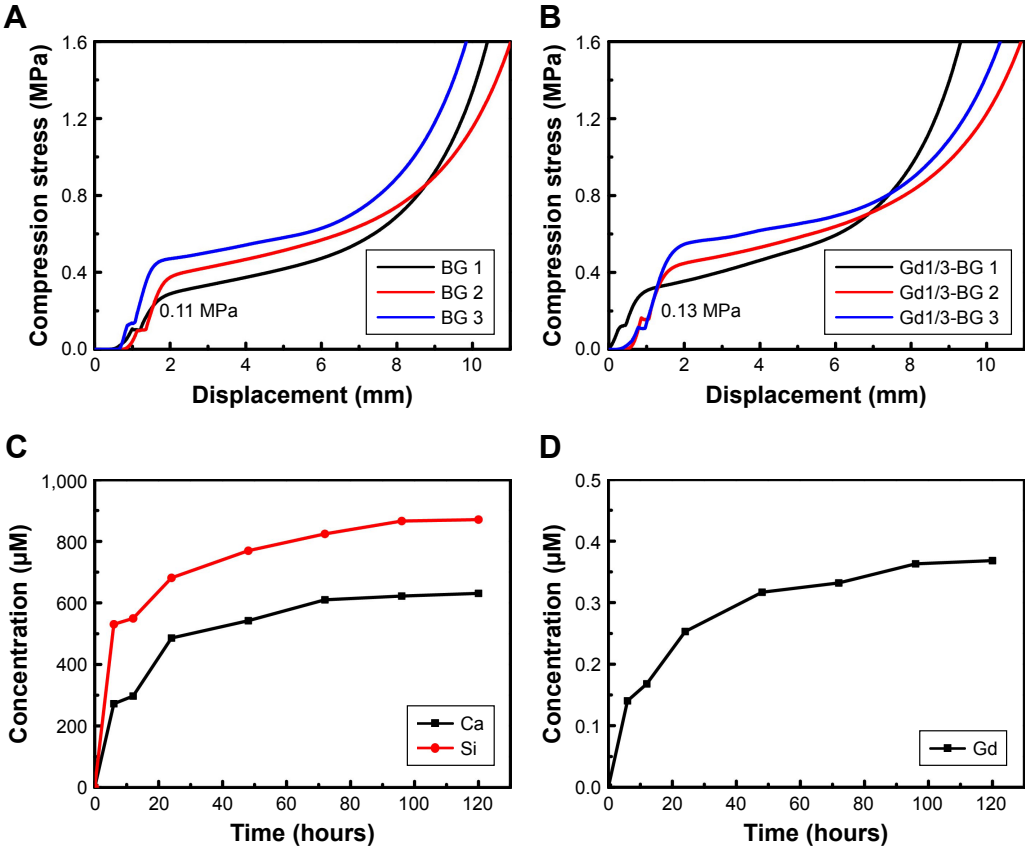

Figure S2 Mechanical property and ion release kinetics of scaffolds.
Notes: Compression strengths of different samples: (**A**) BG scaffolds; (**B**) Gd1/3-BG scaffolds. Ion release performances of Gd1/3-BG scaffolds: (**C**) Ca and Si ions; (**D**) Gd ions.
Abbreviations: BG, bioglass; Gd, gadolinium.